Journal of Physics and Chemistry of Solids 128 (2019) 325–330

Contents lists available at ScienceDirect

Journal of Physics and Chemistry of Solids

journal homepage: www.elsevier.com/locate/jpcs

Moiré superlattices and 2D electronic properties of graphite/MoS_2 heterostructures

Daniel J. Trainer [a], Aleksei V. Putilov [a,1], Baokai Wang [b], Christopher Lane [b], Timo Saari [c], Tay-Rong Chang [e], Horng-Tay Jeng [e,f], Hsin Lin [d,g], Xiaoxing Xi [a], Jouko Nieminen [b,c], Arun Bansil [b], Maria Iavarone [a,*]

[a] Physics Department, Temple University, Philadelphia, PA, 19122, USA
[b] Physics Department, Northeastern University, Boston, MA, 02115, USA
[c] Department of Physics, Tampere University of Technology, Tampere, Finland
[d] Centre for Advanced 2D Materials and Graphene Research Centre, National University of Singapore, Singapore, 117546, Singapore
[e] Department of Physics, National Tsing Hua University, Hsinchu, 30013, Taiwan
[f] Institute of Physics, Academia Sinica, Taipei, 11529, Taiwan
[g] Department of Physics, National University of Singapore, Singapore, 117546, Singapore

A B S T R A C T

Heterostructures of graphite/MoS_2 display a wide range of lattice registry due to rotational alignment and/or lattice mismatch. Using high resolution scanning tunneling microscopy and spectroscopy (STM/STS) we investigated electronic properties of these heterostructures and observed changes in the bandgap as a function of the twist angle between the layers. Green's function based electronic structure calculations were carried out in order to shed light on the mechanism underlying the observed bandgap changes. Indirect coupling between the p_z orbitals of the substrate Carbon atoms and the d_{z2} orbitals of the MoS_2 layers (mediated by the p_z orbitals of the bottom S layers) is found to be responsible for changes in the valence-band edge. Simple stacking of van der Waals materials with diverse properties have the potential to enable the fabrication of novel materials and device structures with tailored electronic properties.

1. Introduction

Artificial van der Waals heterostructures hold the unique promise of combining materials with diverse properties [1,2] to enable the fabrication of novel materials and devices with controlled atomic interfaces [3–7]. In these heterostructures, interactions between the planes of different materials are expected to modify the electronic properties of the constituent materials. In this connection, the influence of interlayer interaction in transition metal dichalcogenides (TMDCs) has been extensively discussed since properties of TMDCs change substantially in going from the monolayer to the bulk material. In the case of MoS_2, for example, there is a transition from an indirect band gap in the bulk to a direct band gap at monolayer [8,9] that can be tuned by functionalization or purposeful tweaking, opening up the possibility of flexible electronics applications [10,11] and field effect transistors [12,13]. Moreover, the spin-orbit-coupling induced spin-split valence bands around the K-points together with a large direct band gap [14], make MoS_2 a promising material for spin/valley electronics. It has been demonstrated that the bandgap decrease of MoS_2 with increasing number of layers is mostly due to a valence-band-edge shift and that the interfacial S atoms are mainly responsible for driving these changes in the band structure [15]. Thus, not surprisingly, there is increasing interest in how interlayer interactions affect properties of the related heterostructures as well [16–18].

Here we report direct measurements of the quasiparticle band gap by varying the relative crystallographic angle between the van der Waals layers of the MoS_2/HOPG heterostructure using scanning tunneling microscopy/spectroscopy (STM/STS). To date, measurements on such heterostructures have been mostly carried out using optical methods [16] or ARPES [19], which are limited in providing a direct window on the nature of valence and conduction band edges. Rotation between adjacent layers in van der Waals structures produces superlattices that provide an interesting model system for gaining insight at the atomic scale into how electronic properties evolve through the rearrangement of atoms in a heterostructure and the factors responsible for superlattice formation. We identify five Moiré superstructures in monolayer MoS_2/HOPG

* Corresponding author.
E-mail address: iavarone@temple.edu (M. Iavarone).
[1] Present address: Institute for Physics of Microstructures RAS, Nizhny Novgorod, GSP-105, 603950, Russia.

https://doi.org/10.1016/j.jpcs.2017.10.034
Received 18 August 2017; Accepted 22 October 2017
Available online 24 November 2017

domains and measure and analyze their band gap values. Changes in the band gap are found to be correlated with Moiré lattice periodicity, indicating a relationship between the Moiré pattern and interlayer coupling. Parallel theoretical modeling using Green's function techniques within a tight-binding (TB) framework are used to unfold the mechanism responsible for producing changes in the bandgap as a function of the twist angle. We thus show that the coupling of the p_z orbital of the substrate Carbon and the d_{z2} orbital of the MoS_2 layer is responsible for driving these changes.

2. Experimental details

Mono- to few-layer thick MoS_2 islands were grown using the well-known ambient pressure chemical vapor deposition technique with ultra-high-purity N_2 (250sccm) as the carrier gas. HOPG substrates were cleaved with scotch tape just prior to loading in the furnace and suspended facedown above ~15 mg of MoO_3 (≥99.5% Sigma Aldrich) in a crucible placed downstream from a different crucible containing 80 mg of Sulphur (≥99.5% Sigma Aldrich). Each crucible was placed in a different heating zone in a 1″ furnace. Temperatures in these two zones were individually controlled using two adjacent tube furnaces. The furnace containing the MoO_3 and HOPG was degassed at 150 °C for 90 min then ramped to 700 °C at a rate of 15 °C/min. Once this furnace reached 320 °C, the furnace containing the Sulphur crucible was ramped to 120 °C at approximately 3 °C/min. Both furnaces were allowed to sit at their maximum temperatures for 30 min at which point the MoO_3 furnace was ramped down at 8 °C/min. Once this furnace reached 580 °C, both furnaces were rapidly cooled to room temperature. This growth method yields monolayer and bilayer MoS_2 domains with varying crystallographic orientations relative to the underlying HOPG substrate [15,20]. Furthermore, this technique ensures a pristine interface between the layers of the heterostructures and is thus advantageous over using chemical transfer or stamping techniques, which necessarily compromise the interface.

Scanning tunneling microscopy/spectroscopy measurements were carried out using a Unisoku STM with PtIr tip in an ultra-high vacuum ($<10^{-11}$ Torr) at T = 4.2 K. Prior to measurements, all samples were degassed at approximately 300 °C and 10^{-10} Torr for a minimum of 3 h up to 10 h, and subsequently moved to the scanner without breaking the vacuum. STM images were recorded in constant current mode with tunneling current of 50–100 pA, 30–50 I–V curves were acquired at each location, and curves from different locations within the same layer were averaged to obtain the dI/dV conductance spectra by numerical derivative.

3. Scanning tunneling microscopy/spectroscopy characterization

Fig. 1 (a–e) shows atomic STM images acquired in constant current mode from five MoS_2 monolayer domains at different twist angles between 0 and 30° with respect to the underlying HOPG substrate. Each image exhibits a different Moiré superstructure reflecting the lattice mismatch between MoS_2 and graphite and the relative angle between the layers [21]. Periodicity of the Moiré pattern is highlighted with blue circles in the 2D fast Fourier transform (FFT) of each topography image in Fig. 1(f)–(j). These FFTs show an inner pattern of peaks which form a hexagon (highlighted in blue) at an angle with respect to the primary peaks of the atomic lattice (white hexagon). The angle between the S-S direction and the graphite direction can be directly measured by acquiring atomic resolution images on the exposed graphite surface. 2D and 3D cartoons of Fig. 2(a)–(c) show the registry between the bottom Sulphur atoms of the MoS_2 and the top Carbon atoms of the HOPG at different relative twist angles. From a strictly geometrical perspective, the Moiré pattern periodicity evolves with twist angle as a monotonic decrease represented by the blue curve in Fig. 2(f) [21]:

$$L(\vartheta) = \frac{a_{HOPG}}{\sqrt{1 + \left(\frac{a_{HOPG}}{a_{MoS2}}\right)^2 - 2\left(\frac{a_{HOPG}}{a_{MoS2}}\right)cos\vartheta}}$$

where L is the Moiré lattice periodicity, a_{HOPG} and a_{MoS2} are the lattice parameter of the graphite and the MoS_2, respectively, and ϑ is the twist angle. This yields L = 1.1 nm at θ = 0, consistent with our experimental observations. In a physical system, however, the Moiré pattern will assume the most energetically favorable configuration as has been seen in STM studies of graphene on transition metal surfaces [22]. Therefore, we should not expect experimental data to adhere to the geometrically derived curve in Fig. 2(f), which represents possible energetically favorable structures for various twist angles.

STM/STS allows us to determine the intrinsic one-electron quasiparticle gap by measuring the local electronic density of states (proportional to the conductance spectrum dI/dV, effects of tunneling matrix

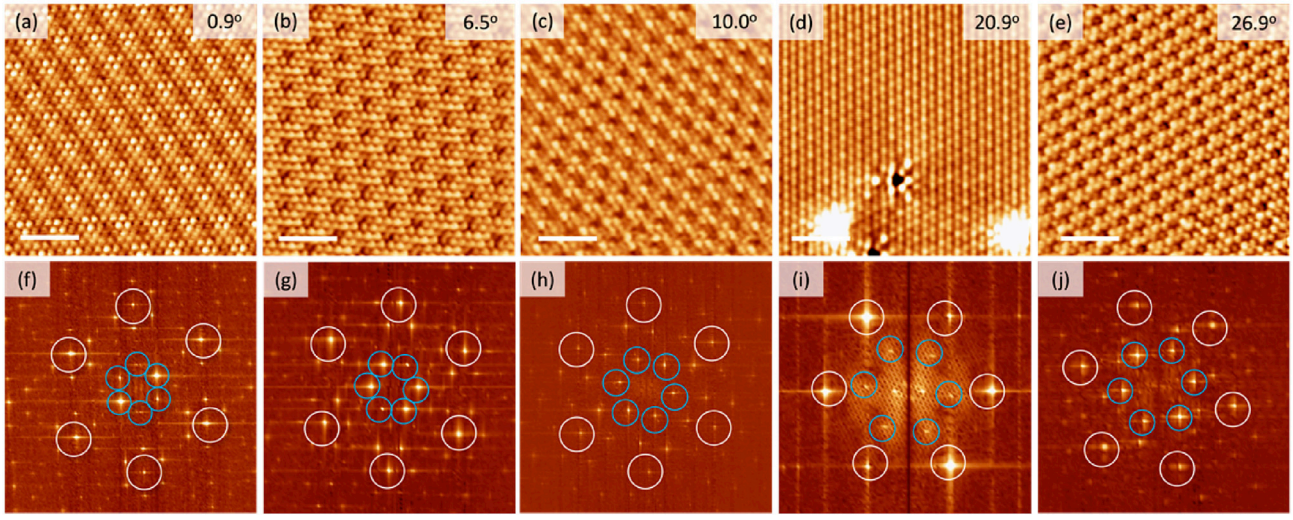

Fig. 1. (a)–(e) Constant-current scanning-tunneling-microscopy images of Moiré patterns of five different domains of single layer MoS_2 for varying angles with respect to the underlying HOPG substrate (V ranging from −0.6 V to −1.5 V, I ranging from 30 pA to 100 pA). Scale bars represent 2 nm. (f)–(j) Fourier transform images corresponding to (a)–(e). Peaks related to the MoS_2 lattice and the Moiré pattern lattice are identified by white and blue circles, respectively. (For interpretation of the references to colour in this figure legend, the reader is referred to the web version of this article.)

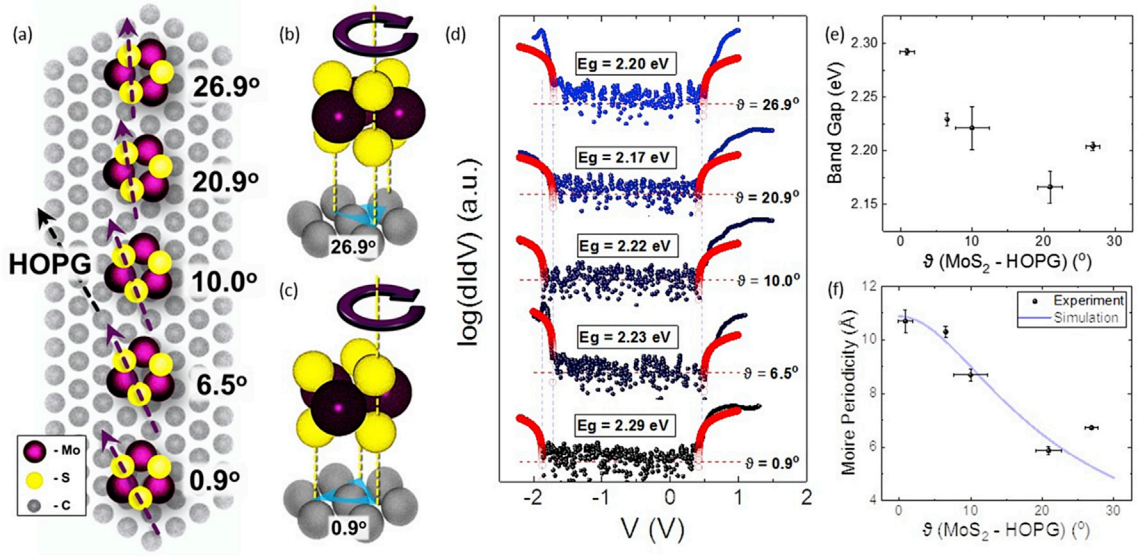

Fig. 2. (a) A 2D cartoon depiction of various measured twist angles of single layer MoS_2 with respect to the underlying HOPG lattice. (b) and (c) 3D cartoons showing examples of the registry between the bottom Sulphur atoms of the MoS_2 and the top Carbon atoms of the HOPG at twist angles of 26.9° and 0.9°. (d) Plots of the average numerical derivative of the current-voltage curves for various twist angles in Fig. 1; the associated gaps are given. (e) Summary plot based on the data of (d) showing gap vs. twist angle. (f) Moiré lattice constant as a function of the twist angle.

element notwithstanding), and correlate it with the local environment at the atomic scale. Representative dI/dV spectra for the five observed Moiré patterns are shown in Fig. 2(d). Several different locations were sampled for each domain, and the averaged I–V spectra were used to obtain the numerical derivative. Results are plotted on a logarithmic scale to highlight edges of the valence band maximum and the conduction band minimum. The gap edges have been determined by making a linear fit to the data within a voltage window at each edge; error is estimated by varying the voltage window over which the linear fit is made. The asymmetry of the spectra around E_F suggests that our films are n-doped, which is typical of films fabricated by CVD [15,23–25]. The quasiparticle bandgap is plotted as a function of the twist angle in Fig. 2(e). A reduction of the band gap is seen with increasing twist angle, which is due mainly to a shift of the valence band maximum. Notably, these variations in the bandgap are similar to those of the Moiré lattice constant with twist angle, suggesting a close relationship between the periodicity of the Moiré lattice and the changes observed in electronic properties (Fig. 2(e) and (f)). Insight into these results can be obtained by considering the atomic registry between the film and substrate at varying twist angles. In particular, our analysis reveals that intensity maxima in the Moiré lattice correspond approximately to coincidences in positions of Sulphur atoms of the MoS_2 layer and Carbon atoms of the adjacent graphite layer or to cases where the distance between these atoms reaches a minimum. This point is clarified in the schematic cartoons of Fig. 2(b) and (c) where a Sulphur atom is positioned above a Carbon atom for the 26.9° twist whereas in the 0.9° case all three Sulphur sites are located between the Carbon atoms. Previous reports of density-functional-theory (DFT) studies of MoS_2/graphene have shown that atomic registry is instrumental for obtaining interfacial electronic transfer, which affects the Mo—S bond length and hence the band structure [26]. As the Moiré periodicity decreases, the number of 'coincident' points per unit area increases, enhancing the coupling between the film and substrate. These considerations indicate that the quasiparticle bandgap is related to the strength of the interlayer interaction in the monolayer MoS_2/graphite system.

4. Theoretical modeling and analysis

We turn now to discuss the nature of the bandgap (direct vs. indirect) and the underlying orbitals involved in terms of our parallel electronic structure computations. In order to create a practical simulation cell, we model the HOPG substrate with a single graphene layer. Furthermore, modeling the effect of the substrate on the electronic structure of the MoS_2 monolayer at an arbitrary twist angle requires a huge simulation cell, and for this reason, we have taken an indirect approach for understanding the relationship between the nature of the band gap and the observed Moiré patterns. In this connection, we take the effective coordination number (ECN) between the Carbon atoms of the graphene nanolayer (GNL) and the lowest layer of Sulphur atoms as an important parameter. Experimentally observed periodicity of Moiré patterns with twist angles can be related to ECN as we noted already, while in our theoretical simulations, we capture effects of ECN by varying the distance between the GNL and the MoS_2 overlayer; a decrease (increase) in ECN can be simulated by increasing (decreasing) this distance since Hamiltonian matrix elements, which involve overlaps of orbital basis functions, vary inversely with distance.

In order to identify the direct vs indirect nature of the band gap, we use two geometries: (1) A MoS_2 overlayer with the same alignment as the underlying graphene substrate (direct gap at K-point), and (2) A MoS_2 overlayer with a 30° twist angle with respect to the graphene substrate (indirect gap from Γ to K point), i.e. the zig-zag direction of MoS_2 is aligned with the armchair direction of graphene. In the former case, 4×4 2D primitive cells of MoS_2 fit in a supercell of 3×3 2D primitive cells of graphene, while in the latter case, the supercell contains 4×4 MoS_2 and 5×5 graphene primitive cells. This basic geometry is used for both first-principles and tight-binding band structure calculations and the associated orbital projections and off-diagonal elements of the density matrix. In Fig. 3(a) and (b) we show the geometry of the two configurations; the corresponding band structures are shown in Fig. 3(c) and (d), respectively.

While our theoretical results are based mainly on computations carried out within the tight-binding framework, we emphasize that we have used material specific tight-binding parameters, which have been obtained via the corresponding first-principles calculations. For this purpose, we used the projector augmented-wave method [27] as implemented in the Vienna Ab Initio Simulation Package (VASP) [28,29] within the framework of the DFT. The PBE-pseudopotential [30] and DFT-D2 method [31] for treating van der Waals interactions were used. Spin-orbit coupling (SOC) was included in self-consistency cycles and band computations. Tight-binding parameters for MoS_2 were fitted to

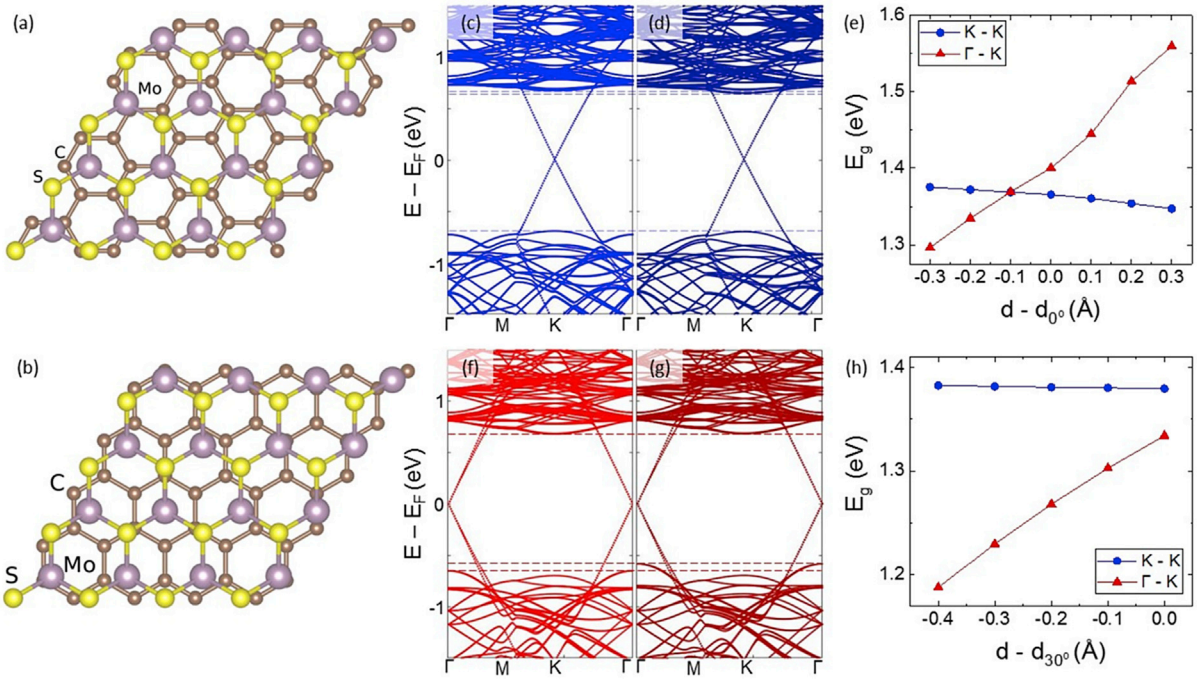

Fig. 3. Ball and stick models of (a) 0° and (b) 30° configuration. Band structure for the 0° case at the unperturbed structure (c) and for the structure with graphene–overlayer distance increased by 0.4 Å (d). (e) Band gap values (Eg) of the direct gap (blue) and the indirect gap (red) as a function of the graphene–overlayer distance d relative to the unperturbed distance d_0 for the 0° case. Band structure for the 30° case at the unperturbed structure (f) and for the structure in which the graphene–overlayer distance has been compressed by 0.4 Å (g). (h) Band gap values (Eg) of the direct gap (blue) and the indirect gap (red) as a function of the graphene–overlayer distance d relative to the unperturbed distance d_{30} for the 30° case. (For interpretation of the references to colour in this figure legend, the reader is referred to the web version of this article.)

Slater-Koster-type matrix-element form as in our earlier work [15]. Amplitudes of Slater-Koster terms for graphene and graphene–Sulphur interactions were fitted to correctly reproduce the direct–indirect gap transition in going from the 0° to 30° rotated configuration.

Our basic building block for modeling the geometry of the system is the 2D primitive cell of a single MoS_2 layer, which contains one Mo and two S atoms. Two spin degrees of freedom are included for each orbital with S atoms modeled with one s- and three p-orbitals, and Mo with one s- and five d-orbitals. For the graphene substrate, we use one s- and three p-orbitals for each C atom. As a result, our supercell has 4 × 4 primitive cells each having 2 × 14 orbitals in a monolayer MoS2 film. In addition, the supercell of the heterostructure includes 5 × 5 or 3 × 3 unit cells each with 2 × 4 orbitals of the graphene layer depending on the twist angles of 0° or 30°.

We cast our TB Hamiltonian in the following form [32,33]:

$$H = \sum_{\alpha\beta\sigma}\left(\varepsilon_\alpha c^\dagger_{\alpha\sigma}c_{\alpha\sigma} + V_{\alpha\beta}c^\dagger_{\alpha\sigma}c_{\beta\sigma}\right) + H_{SOC} \tag{1}$$

where ε_α is the onsite energy of orbital α, σ is the spin index and $V_{\alpha\beta}$ is the hopping integral between orbitals α and β. H_{SOC} takes into account SOC-effects between the onsite Mo d-orbitals (much weaker SOC terms for S atoms are neglected) and has the form [34]:

$$H_{SOC} = \alpha L\cdot\sigma \tag{2}$$

where L denotes orbital angular momentum, and the parameter α is fitted to reproduce the spin-orbit splitting found in the ab-initio band structure. The SOC part of the Hamiltonian [35] can be cast as:

$$H_{SOC} = \sum_{i,j}\alpha\left(c^\dagger_{p_i\uparrow}, c^\dagger_{p_i\downarrow}\right)\left(\sigma\cdot u_i \times u_j\right)\left(c_{pi\uparrow}, c_{pi\downarrow}\right)^T$$

where i and j denote directions (x, y, z), p_i and p_j refer to p-orbitals of the same atom, and $\boldsymbol{u}_i$ is a unit vector pointing in the direction of the ith orbital. Our tight-binding model is constructed to reproduce the DFT band structure at the edges of valence and conduction bands, as well as the graphene bands within the gap and their behavior close to the valence band edge, which are of main interest to this study. In order to unfold the mechanism behind Moiré pattern formation, we capture effects of the ECN by varying the interlayer distance between graphene and MoS_2, which changes the amplitude of the overlap terms between Carbon and Sulphur orbitals in our Hamiltonian.

We next construct the Green's function based on the Hamiltonian of Eq. (1) in which many-body corrections and external interactions are introduced via a self-energy matrix Σ [36–40]:

$$G(E,k) = [E - H(k) - \Sigma(E,k)]^{-1} \tag{3}$$

Here we use the simplest possible approximation for Σ to represent an inelastic background, $\Sigma = -i\eta$, where η is a small (real) positive parameter.

The Green's function matrix in Eq. (3) gives the density matrix:

$$\rho(E,k) = \frac{1}{2\pi i}\left(G(E,k) - G(E,k)^\dagger\right) \tag{4}$$

The matrix elements, $\rho_{\alpha\sigma\beta\sigma'}(E,k)$, of the density matrix allow the computation of spin/orbital projections of the band structure. The 0° and 30° configurations we considered for the alignment of MoS_2 on graphene are considered in Fig. 3(a) and (b). Moiré patterns are observed with an angle-dependent periodicity that reflects the commensurate alignment between the GNL and the overlayer, which in turn is related presumably to the effective coordination number of the Sulphur atoms at the interface with respect to the Carbon atoms of the graphene substrate. This coordination number is inversely proportional to the distance d between the overlayer and GNL. Instead of creating impractically large supercells for small rotation angles, we vary the interlayer distance d perturbatively as a way of capturing the behavior of the band gap.

Effects of change in the graphene-overlayer distance between the 0° and 30° configurations can be delineated with reference to Fig. 3.

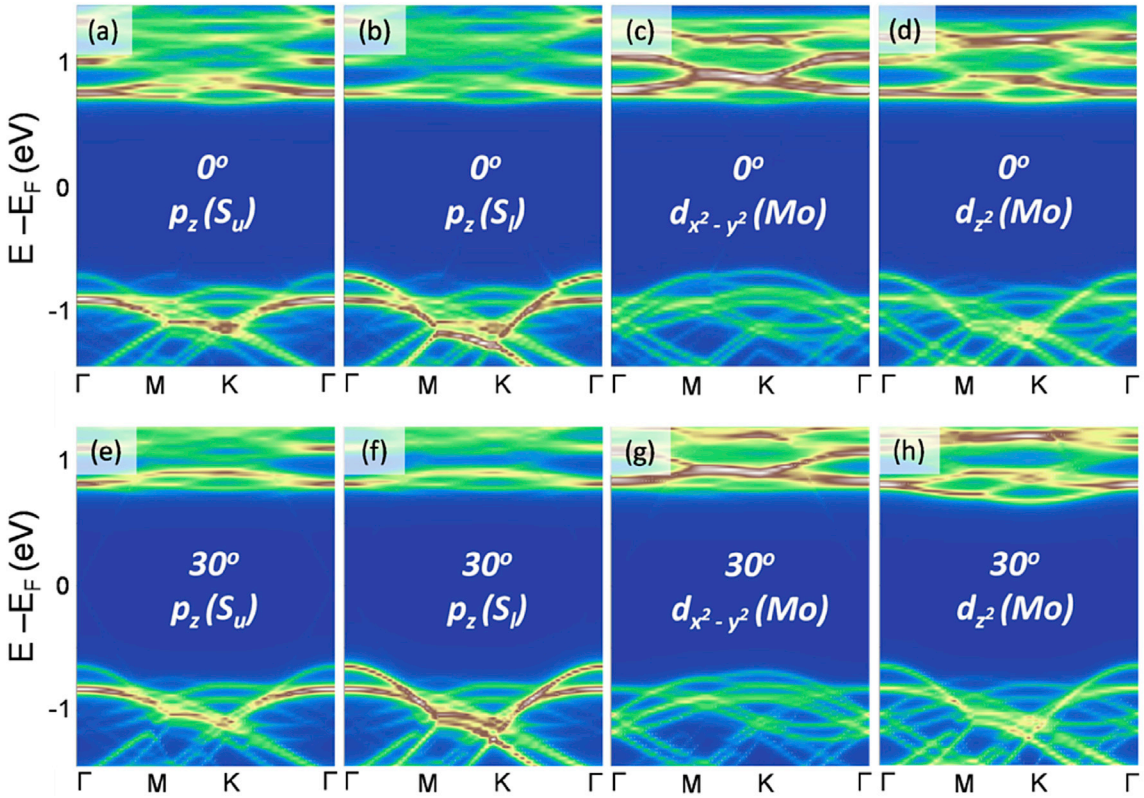

Fig. 4. Contribution to the band structure for the 0° case from various orbitals as follows: (a) p_z of the upper-layer Sulphur (S_u); (b) p_z of the lower-layer Sulphur (S_l); (c) $d_{x2\text{-}y2}$ of Molybdenum; and, (d) d_{z2} of Molybdenum. (e)–(h) Same as (a)–(d) except that these panels refer to the corresponding 30° cases.

Band structures of Fig. 3(c) and (f) show that the band gap changes from direct to indirect in going to the 30° configuration due to an upward shift of valence states at the Γ-point. Fig. 3(d) shows the band structure at 0° corresponding to an increased graphene-overlayer distance of 0.4 Å. The increased interlayer distance mostly affects valence states at Γ along with a slight lowering of the conduction states at K, so that the gap remains direct at K with a reduced size, see Fig. 3(e). This is consistent with the reduced experimental gap observed in moving away from the 0° configuration. In the 30° configuration the main effect of reducing the graphene-overlayer distance is an upward movement of valence states at Γ (Fig. 3(g)) along with a reduction of the indirect gap, see Fig. 3(h). This is consistent with the behavior of the reduced experimental gap moving away from 30° towards smaller angles.

The origin of preceding changes in the bandgap can be understood from the results of Fig. 4, where contributions to the unperturbed band structures from various orbitals for the 0° (panels (a)–(d)) and 30° (panels (e)–(h)) configurations are shown. The dominant orbitals contributing to the top of the valence band at K are $d_{x2\text{-}y2}$ or d_{xy} (Fig. 4(c), (d), (g) and (h)) and, because these orbitals have little overlap with p_z orbitals, they are not sensitive to Sulphur orbitals. On the other hand, p_z-orbitals of both the upper (Fig. 4(a) and (e)) and lower Sulphur atoms (Fig. 4(b) and (f)) contribute to the top of the valence band at Γ, and the spectral weight of the interface Sulphur atoms is emphasized through its overlap with p-orbitals of Carbon atoms of the graphene layer. Symmetry of d_{z2}-orbitals of Molybdenum and their extension along the z-direction help mediate changes in graphene-Sulphur overlap and provide a tunneling channel to the surface.

A more quantitative analysis of the dependence of the band gap on the graphene-Sulphur distance is shown in Fig. 3(e) and (h). We see in Fig. 3(e) for the unperturbed configuration that the direct gap would change to indirect with a decrease of about 0.15 Å in the interlayer distance. Fig. 3(h) for the 30° configuration, on the other hand, shows that the indirect band gap is more sensitive to the interlayer distance than the direct gap at K. This is to be expected since valence states at K are mainly due to $d_{x2\text{-}y2}$ orbitals, which are insensitive to graphene-Sulphur overlap.

5. Summary and conclusions

We have investigated heterostructures of graphite/MoS_2 in order to understand the evolution of electronic properties of the heterostructure through the rearrangement of atoms when the monolayer MoS_2 is twisted with respect to the underlying graphite substrate. For this purpose, we carried out low-temperature STM/STS measurements for five different values of the twist angle varying from zero to 30°. Experimentally observed changes in band gaps were analyzed via parallel electronic structure computations within the framework of tight-binding Hamiltonians where the overlap parameters were derived from first-principles band structures. For small variations in the twist angle around zero and 30°, where the size of the supercell becomes impractically large, we modeled the electronic structure by varying the distance between the substrate and the overlayer as a perturbation. Our analysis shows that the band gap changes from direct to indirect in going from zero to 30° twist angle due to an upward shift of valence states at the Γ-point. The dominant orbital contributing to the top of the valence band at the K-point is found to be $d_{x2\text{-}y2}$ (or d_{xy}), while p_z-orbitals of both the lower and upper Sulphur atoms contribute to the top of the valence band at the Γ-point. Our study provides insight into how the electronic structure of heterostructures could be tuned through rotational alignment of layers as a control parameter for applications.

Acknowledgements

It is a pleasure to acknowledge important conversations with Adrienn Ruzsinszky, Qimin Yan and Liping Yu. This work was supported primarily

by the Center for the Computational Design of Functional Layered Materials (CCDM), an Energy Frontier Research Center funded by the U.S. Department of Energy, Office of Science, Basic Energy Sciences under Award #DE-SC0012575 (STM measurements and thin-film growth). It benefited from resources of the Institute of Advanced Computing, Tampere. T.S. is grateful to Väisälä Foundation for financial support. H.L. acknowledges the Singapore National Research Foundation for support under NRF Award No. NRF-NRFF2013-03. The work at Northeastern University was supported by the US Department of Energy (DOE), Office of Science, Basic Energy Sciences grant number DEFG02-07ER46352 (core research), and benefited from Northeastern University's Advanced Scientific Computation Center (ASCC), the NERSC supercomputing center through DOE grant number DE-AC02-05CH11231, and support (applications to layered materials) from the CCDM under DE-SC0012575.

References

[1] A.K. Geim, I.V. Grigorieva, Nature 449 (2013) 419.
[2] G.H. Gao, W. Gao, E. Cannuccia, J. Taha-Tijerina, L. Balicas, A. Mathkar, T.N. Narayanan, Z. Liu, B.K. Gupta, J. Peng, Y.S. Yin, A. Rubio, P.M. Ajayan, Nano Lett. 12 (2012) 3518.
[3] J. Yoon, W. Park, G.-Y. Bae, Y. Kim, H.S. Jang, Y. Hyun, S.K. Lim, Y.H. Kahng, W.-K. Hong, B.H. Lee, H.C. Ko, Small 9 (2013) 3295.
[4] T. Roy, M. Tosun, J.S. Kang, A.B. Sachid, S.B. Desai, M. Hettick, C.C. Hu, A. Javeyet, ACS Nano 8 (2014) 6259.
[5] C.R. Dean, A.F. Young, I. Meric, C. Lee, L. Wang, S. Sorgenfrei, K. Watanabe, T. Taniguchi, P. Kim, K.L. Shephard, J. Hone, Nat. Nanotechnol. 5 (2010) 722.
[6] L. Britnell, R.V. Gorbachev, R. Jalil, B.D. Belle, F. Schedin, A. Mishchenko, T. Georgiou, M.I. Katsnelson, L. Eaves, S.V. Morozov, N.M.R. Peres, J. Leist, A.K. Geim, K.S. Novoselov, L.A. Ponomarenko, Science 335 (2012) 947.
[7] A. Vargas, F. Liu, C. Lane, D. Rubin, I. Bilgin, Z. Hennighausen, M. Decapua, A. Bansil, S. Kar, Sci. Adv. 3 (2017) e1601741.
[8] A. Kuc, N. Zibouche, T. Heine, Phys. Rev. B 83 (2011), 245213.
[9] K.F. Mak, C. Lee, J. Hone, J. Shan, T.F. Heinz, Phys. Rev. Lett. 105 (2010), 136805.
[10] Q.H. Wang, K. Kalantar-Zadeh, A. Kis, J.N. Coleman, M.S. Strano, Nat. Nanotechnol. 7 (2012) 699.
[11] B. Radisavljevic, M.B. Whitwick, A. Kis, ACS Nano 5 (2011) 9934.
[12] B. Radisavljevic, A. Radenovic, J. Brivio, V. Giacometti, A. Kis, Nat. Nanotechnol. 6 (2011) 147.
[13] Z. Yin, H. Li, L. Hone, L. Jiang, Y. Shi, Y. Sun, G. Lu, Q. Zhang, X. Chen, H. Zhang, ACS Nano 6 (2011) 74.
[14] T.-R. Chang, H. Lin, H.-T. Jeng, A. Bansil, Sci. Rep. 4 (2014) 6270.
[15] D.J. Trainer, A.V. Putilov, C. Di Giorgio, T. Saari, B. Wang, M. Wolak, R.U. Chandrasena, C. Lane, T.-R. Chang, H.-T. Jeng, H. Lin, F. Kronast, A.X. Gray, X.X. Xi, J. Nieminen, A. Bansil, M. Iavarone, Sci. Rep. 7 (2017) 40559.
[16] H. Fang, C. Battaglia, C. Carraro, S. Nemsak, B. Ozdol, J.S. Kang, H.A. Bechtel, S.B. Desai, F. Kronast, A.A. Unal, G. Conti, C. Conlon, G.K. Palsson, M.C. Martin, A.M. Minor, C.S. Fadley, E. Yablonovitch, R. Maboudian, A. Javey, PNAS 111 (2014) 6198.
[17] N. Alidoust, G. Bian, S.Y. Xu, R. Sankar, M. Neupane, C. Liu, I. Belopolski, D.X. Qu, J.D. Denlinger, F.C. Chou, M.Z. Hasan, Nat. Commun. 5 (2014) 4673.
[18] X.D. Li, S. Yu, S.Q. Wu, Y.H. Wen, S. Zhou, Z.Z. Zhu, J. Phys. Chem. C 117 (2013) 15347.
[19] H.C. Diaz, J. Avila, C. Chen, R. Addou, M.C. Asensio, M. Batzill, Nano Lett. 15 (2015) 1135.
[20] Y.H. Lee, X.-Q. Zhang, W. Zhang, M.-T. Chang, C.-T. Lin, K.-D. Chang, Y.-C. Yu, J.T.-W. Wang, C.-S. Chang, L.-J. Li, T.-W. Lin, Adv. Mater 24 (2012) 2320.
[21] P. Zeller, S. Gunther, New J. Phys. 16 (2014) 83028.
[22] P. Merino, M. Svec, A.L. Pinardi, G. Otero, J.A. Martin-Gago, ACS Nano 5 (2011) 5627.
[23] C. Zhang, A. Johnson, C.L. Hsu, L.J. Li, C.K. Shih, Nano Lett. 14 (2014) 2443.
[24] Y.L. Huang, Y. Chen, W. Zhang, S.Y. Quek, C.-H. Chen, L.-L. Li, W.-T. Hsu, W.-H. Chang, Y.J. Zheng, W. Chen, A.T.S. Wee, Nat. Commun. 6 (2015) 6298.
[25] H. Schmidt, S. Wang, L. Chu, M. Toh, R. Kumar, W. Zhao, A.H. Castro Neto, J. Martin, S. Adam, B. Özyilmaz, G. Eda, Nano Lett. 14 (2014) 1909.
[26] A. Ebnonnasir, B. Narayanan, S. Kodambaka, C.V. Ciobanu, Appl. Phys. Lett. 105 (2014) 31603.
[27] P.E. Blöchl, Phys. Rev. B 50 (1994) 17953.
[28] G. Kresse, J. Hafner, Phys. Rev. B 48 (1993) 13115.
[29] G. Kresse, J. Furthmüller, Phys. Rev. B 54 (1996) 11169.
[30] J.P. Perdew, K. Burke, M. Ernzerhof, Phys. Rev. Lett. 77 (1996) 3865.
[31] S. Grimme, J. Comp. Chem. 27 (2006) 1787.
[32] J.C. Slater, G.F. Koster, Phys. Rev. 94 (1954) 1498.
[33] W.A. Harrison, Dover, New York, 1989.
[34] S. Konschuh, M. Gmitra, J. Fabian, Phys. Rev. B 82 (2010), 245412.
[35] T.H. Hsieh, H. Lin, J. Liu, W. Duan, A. Bansil, L. Fu, Nat. Comm. 3 (2012) 982–987.
[36] A.L. Fetter, J.D. Walecka, Dover, New York, 2003.
[37] M. Paulsson, M. Brandbyge, Phys. Rev. B 76 (2007), 115117.
[38] A.P. Horsfield, A.M. Bratkovsky, M. Fearn, D.G. Pettifor, M. Aoki, Phys. Rev. B 53 (1996) 12694.
[39] T. Das, R.S. Markiewicz, A. Bansil, Phys. Rev. B 81 (2010), 174504.
[40] J. Nieminen, I. Suominen, T. Das, R.S. Markiewicz, A. Bansil, Phys. Rev. B 85 (2012), 214504.